J. Fluid Mech. (2006), *vol.* 548, *pp.* 431–443.
doi:10.1017/S0022112005007755 Printed in the United Kingdom

Shear flow and viscosity in single-layer hydraulics

By ANDREW McC. HOGG AND GRAHAM O. HUGHES

Research School of Earth Sciences, The Australian National University, Canberra, ACT, 0200, Australia

(Received 6 April 2005 and in revised form 10 August 2005)

We calculate solutions for one-layer hydraulically controlled flows with viscosity. Viscosity and bottom drag produce two key modifications to inviscid hydraulic theory: the position of the hydraulic control point is altered, and the solution requires knowledge of the velocity profile over the entire domain. Hence, analytically tractable solutions are not generally possible and a numerical technique is developed to calculate such flows.

In this paper, bottom drag and fluid viscosity are treated as independent parameters, allowing the influence of each parameter on flux, flow dissipation and position of hydraulic control to be quantified. We find that the flow is determined primarily by the bottom drag, and, surprisingly, the largest perturbation from this state occurs for intermediate values of fluid viscosity.

1. Introduction

Hydraulic theory is commonly used to predict density-driven flows over sills and through channels. The application of this theory is underpinned by the concept of hydraulic control, in which the flow field adjusts to a well-defined state at one or more discrete points in the flow. The flow is termed critical at these *control points*, corresponding physically to points at which the speed of long waves vanishes. To apply hydraulic theory one must first determine the position of the control points. The solution of a reduced set of governing equations at the control points is then sufficient to specify the entire flow field.

Hydraulic techniques have the advantage that they provide a simplified (and often analytically tractable) solution to a nonlinear flow problem. However, they can only be used if one is willing to make a number of simplifying assumptions about the flow. For example, traditional hydraulic theory is steady, inviscid, non-diffusive and hydrostatic (e.g. Armi 1986). All of these assumptions are violated in most geophysical applications of hydraulic theory; yet theoretical predictions both provide reasonable estimates of flux and contribute towards our understanding of the physics of such flows.

Attempts have been made to extend hydraulic theory to incorporate friction and viscosity (as well as diffusion and non-hydrostatic effects). For example, Pratt (1986) demonstrated that for hydraulically controlled one-layer flow over a sill, the addition of bottom drag reduces the flux (assuming that upstream height remains constant) and shifts the control point downstream of the sill (compared with the inviscid case in which the control point is at the top of the sill). However, Pratt's conclusions were based on the assumption that the bottom drag is communicated instantly over the

depth of the water column (to give a uniform velocity profile). Garrett & Gerdes (2003) examined how control conditions are modified when velocity varies with depth. They found that the introduction of velocity shear increases the long-wave speed, and that control still corresponds to points where the wave speed matches the mean flow speed. Thus control occurs at greater mean flow speeds. Garrett (2004) used this result to argue that a vertical gradient in horizontal velocity (owing to the distribution of bottom drag through the water column by internal viscosity) shifts the control point back upstream, towards the sill crest. Garrett also predicts that under certain assumptions viscous solutions can be obtained analytically.

Motivated by Garrett (2004) we review the derivation of controlled viscous hydraulics for a single-layer flow with a free surface (§ 2). In § 3 we develop a numerical solution method for single-layer hydraulically controlled flows, under the influence of bottom drag and viscosity. Bottom drag and viscosity (which are physically related in both turbulent and laminar flows) are independently specified in this numerical study, allowing us to study a wide range of parameter space without using an explicit parameterization for turbulence. In addition, by non-dimensionalizing the equations we are able to predict and verify the role of the channel aspect ratio: longer channels amplify the effects of both viscosity and bottom drag. We present results (§ 4) which demonstrate that the simplifying assumptions which make Garrett's solution analytically tractable are not, in general, justifiable, and that this problem can only be solved numerically.

2. Background theory

2.1. *Governing equations*

For steady viscous flow along a channel, with variable width $b(x)$ and variable bottom height $H(x)$, the momentum equation in the x-direction is

$$uu_x + wu_z = -g(H_x + h_x) + (\nu u_z)_z, \tag{2.1}$$

where $h(x)$ is the height of the free surface, $u(x, z)$ is the along-channel fluid velocity (spanwise variations in velocity are assumed small), $w(x, z)$ represents vertical velocity, g is acceleration due to gravity and $\nu(z)$ a vertical viscosity coefficient. We have assumed that pressure is hydrostatic and mass is conserved, or

$$(bu)_x + (bw)_z = 0. \tag{2.2}$$

It is convenient to transform these equations to a coordinate system (X, η) where $X = x$ and η is an upstream height coordinate for a streamline ($\eta = z$ at $X = -L$). This transformation is written (following Killworth 1992; Engqvist & Hogg 2004)

$$\frac{\partial}{\partial x} \to \frac{\partial}{\partial X} - \frac{z_X}{z_\eta}\frac{\partial}{\partial \eta}, \quad \frac{\partial}{\partial z} \to \frac{1}{z_\eta}\frac{\partial}{\partial \eta},$$

and applied to (2.2) with the identity $w = uz_X$ to give

$$(buz_\eta)_X = 0, \tag{2.3}$$

which, upon integration, defines a flux per unit height, Q, that is constant along streamlines

$$Q(\eta) = buz_\eta. \tag{2.4}$$

The coordinate transformation applied to the momentum equation (2.1) yields

$$uu_X = -g\,(H_X + h_X) + \frac{1}{z_\eta}\left(\frac{\nu u_\eta}{z_\eta}\right)_\eta . \tag{2.5}$$

Equations (2.4) and (2.5) describe a system in which vertical friction is important, and lateral friction is negligible. Thus, the results shown here will only strictly apply in cases where the channel is wide relative to its depth, so that sidewall boundary layers are thin, and thus the lateral shear, u_y, is small. In the calculations below we assume free slip conditions on the sidewalls.

2.2. *Controlled flow*

We now apply a similar methodology to Garrett (2004) to find controlled flow in this coordinate system. The layer thickness h may be written

$$h \equiv \int_H^{H+h} \mathrm{d}z = \int_0^{\eta_0} z_\eta \,\mathrm{d}\eta = \int_0^{\eta_0} \frac{Q}{bu}\,\mathrm{d}\eta, \tag{2.6}$$

where the origin of the z-axis is defined by the bottom of the channel at the upstream end, and η_0 is the height of the free surface in streamline coordinates (which corresponds to the free-surface height at the upstream edge of the domain). Here Garrett (2004) used Gill's (1977) functional approach to find hydraulic control; instead we follow an approach similar to Armi (1986) in which the X-derivative of an energy equation is constrained by regularity conditions at control points. Thus we differentiate (2.6) with respect to X,

$$h_X = -\int_0^{\eta_0} \frac{Qu_X}{bu^2}\,\mathrm{d}\eta - \int_0^{\eta_0} \frac{Qb_X}{b^2 u}\,\mathrm{d}\eta, \tag{2.7}$$

and substitute for u_X using (2.4) and (2.5), to give

$$h_X\left(1 - \int_0^{\eta_0} \frac{gQ}{bu^3}\,\mathrm{d}\eta\right) = H_X \int_0^{\eta_0} \frac{gQ}{bu^3}\,\mathrm{d}\eta - \int_0^{\eta_0} \frac{1}{u^2}\left(\frac{\nu u_\eta}{z_\eta}\right)_\eta \mathrm{d}\eta - \frac{hb_X}{b}. \tag{2.8}$$

This relationship is equivalent to that derived by Garrett & Gerdes (2003) for the case of an inviscid shear flow. The regularity conditions are invoked, implying hydraulic control, when the right-hand side of (2.8) is zero, in which case either $h_X = 0$, or a Froude number, $F = 1$. The Froude number is defined from (2.8) as follows:

$$\frac{1}{F^2} \equiv \int_0^{\eta_0} \frac{gQ}{bu^3}\,\mathrm{d}\eta = \int_H^{H+h} \frac{g}{u^2}\,\mathrm{d}z. \tag{2.9}$$

This definition is equivalent to the usual layered Froude number, in that $F^2 \sim u^2/gh$ and the control condition ($F^2 = 1$) describes a state where long waves are arrested.

When viscosity is finite, Garrett (2004) showed that the control condition is unchanged, but that the position of the control is altered such that the following constraint (calculated by setting the bracketed term on the left-hand side of (2.8) to zero) is satisfied:

$$\int_0^{\eta_0} \frac{1}{u^2}\left(\frac{\nu u_\eta}{z_\eta}\right)_\eta \mathrm{d}\eta = H_X - \frac{hb_X}{b}. \tag{2.10}$$

Integrating the left-hand side of (2.10) by parts gives

$$\int_0^{\eta_0} \frac{2\nu u_\eta^2}{u^3 z_\eta}\,\mathrm{d}\eta - C_d = \int_H^{H+h} \frac{2\epsilon}{u^3}\,\mathrm{d}z - C_d = H_X - \frac{hb_X}{b}, \tag{2.11}$$

where ϵ is the dissipation per unit mass. We have assumed that stress at the upper surface is zero, whereas stress at the bottom of the channel is parameterized by a quadratic drag law using $u_0(X)$, the velocity at the bottom of the channel, and a dimensionless drag coefficient C_d:

$$\nu \frac{\partial u}{\partial z}\bigg|_{z=H} = \nu \frac{u_\eta}{z_\eta}\bigg|_{\eta=0} = C_d u_0^2. \tag{2.12}$$

Equation (2.11) demonstrates that the addition of bottom drag shifts the control point downstream of the topographic constriction (where the right-hand side is negative), while internal dissipation returns it back upstream (to less negative values). These control conditions differ from inviscid hydraulics in that the position of control depends upon the velocity shear owing to viscosity (the left-hand side of (2.11), which is non-zero). The viscous contribution may be small in some cases, but we argue below that it prevents specific analytical solutions of the type proposed by Garrett (2004). Thus we aim to calculate solutions numerically.

2.3. *Dimensionless governing equations*

The role of channel length and fluid depth in this problem is examined by introducing the channel aspect ratio. We begin by non-dimensionalizing the equations derived above using the upstream height above the sill ($\eta_0 - H_s$) as the vertical length scale and the upstream channel length L as the horizontal length scale. The velocity scale is then $(g(\eta_0 - H_s))^{1/2}$. Note that there are alternative horizontal and vertical length scales describing the constriction geometry which could be used: we use the numerical experiments to validate *a posteriori* this choice of length scales.

In terms of non-dimensional quantities, designated with a tilde, (2.5) becomes

$$\tilde{u}\tilde{u}_{\tilde{X}} = -(\tilde{H}_{\tilde{X}} + \tilde{h}_{\tilde{X}}) + \frac{1}{ReA\tilde{z}_{\tilde{\eta}}}\left(\frac{\tilde{u}_{\tilde{\eta}}}{\tilde{z}_{\tilde{\eta}}}\right)_{\tilde{\eta}}, \tag{2.13}$$

where $Re \equiv g^{1/2}(\eta_0 - H_s)^{3/2}/\nu$ is the Reynolds number and $A \equiv (\eta_0 - H_s)/L$ is the channel aspect ratio. It can then be shown that the equation for control position (2.11) becomes

$$\frac{2}{ReA}\int_0^1 \frac{\tilde{u}_{\tilde{\eta}}^2}{\tilde{u}^3\tilde{z}_{\tilde{\eta}}}\,\mathrm{d}\tilde{\eta} - \frac{C_d}{A} = \tilde{H}_{\tilde{X}} - \frac{\tilde{h}\tilde{b}_{\tilde{X}}}{\tilde{b}}, \tag{2.14}$$

where the stress at the bottom is parameterized as

$$\frac{\tilde{u}_{\tilde{\eta}}}{\tilde{z}_{\tilde{\eta}}}\bigg|_{\tilde{\eta}=0} = ReC_d\tilde{u}_0^2. \tag{2.15}$$

These equations suggest that the full parameter space can be spanned by varying only viscosity and bottom drag (or equivalently, the two dimensionless parameters $1/ReA$ and C_d/A). Thus, decreasing aspect ratio is equivalent to increasing both viscosity and bottom drag. This is consistent with the scaling proposed by Hogg, Ivey & Winters (2001) for the case of bi-directional exchange flow.

3. Numerical solution

For clarity, we derive the numerical solution method in dimensional parameter space (noting that we return to the dimensionless coordinates to interpret the results). We assume a solution in which the flux per unit height Q is constant (with η) at the

upstream end of the channel, and viscosity ν is uniform. Equation (2.4) can then be used to eliminate z_η in the momentum equation (2.5),

$$u_X = \frac{-g\,(H_X + h_X)}{u} + \frac{\nu b^2}{2Q^2}(u^2)_{\eta\eta}, \tag{3.1}$$

and to rewrite (2.8),

$$h_X\left(\frac{F^2-1}{F^2}\right) = \frac{H_X}{F^2} - \frac{\nu b}{2Q}\int_0^{\eta_0}\frac{(u^2)_{\eta\eta}}{u^2}\,\mathrm{d}\eta - \frac{hb_X}{b}. \tag{3.2}$$

The momentum equation can be integrated with respect to X – this is achieved by first calculating h_X (from (3.2)), and then u_X (3.1). The numerical integration starts from the upstream end of the domain and continues until a control point is reached, where $F^2 = 1$, and

$$\frac{\nu b}{2Q}\int_0^{\eta_0}\frac{(u^2)_{\eta\eta}}{u^2}\,\mathrm{d}\eta = H_X - \frac{hb_X}{b}. \tag{3.3}$$

This technique works in principle, provided the flow is either sub- or supercritical. However, near the control point (3.2) becomes singular. In such cases we use an alternative equation, obtained from differentiating (2.8) and assuming $F^2 \approx 1$ to give a quadratic in $y = (h_X + H_X)$,

$$\left(\frac{3Qg^2}{b}\int_0^{\eta_0}\frac{1}{u^5}\,\mathrm{d}\eta\right)y^2 - \left(\frac{5\nu gb}{2Q}\int_0^{\eta_0}\frac{(u^2)_{\eta\eta}}{u^4}\,\mathrm{d}\eta - \frac{2b_X}{b}\right)y + \frac{\nu^2 b^3}{2Q^3}\int_0^{\eta_0}\frac{((u^2)_{\eta\eta})^2}{u^3}\,\mathrm{d}\eta$$
$$+H_{XX} - \frac{\nu b_X}{2Q}\int_0^{\eta_0}\frac{(u^2)_{\eta\eta}}{u^2}\,\mathrm{d}\eta + \frac{H_X b_X}{b} - \frac{hb_{XX}}{b} + \frac{hb_X^2}{b^2} - \frac{\nu b}{2Q}\int_0^{\eta_0}\frac{(u^2)_{\eta\eta X}}{u^2}\,\mathrm{d}\eta = 0. \tag{3.4}$$

Note that the term which represents the X-derivative of the shear (the last term in (3.4)) is assumed small, and is ignored (this assumption has been confirmed *a posteriori*).

The numerical solution method for this problem involves a shooting algorithm. For a given value of Q the local value of h_X can be calculated from (3.2) (or (3.4) if $F^2 \approx 1$), and (3.1) used to spatially integrate u in X with first-order forward differences. Thus we can integrate along the length of the channel: at the end of the channel, or when $F^2 > 1$, we evaluate the control condition, modify Q and repeat the above procedure. By iterating over Q until the solution satisfies both control conditions, we can find a unique solution.

The numerical algorithm uses variable vertical resolution to allow better simulation of the lower boundary layer. The dependence of results upon vertical resolution (not shown here) demonstrates that the model obtains a smooth convergence of parameters with high resolution. Therefore, we can balance vertical resolution (and hence CPU time) with accuracy: in all experiments 40 gridpoints in the vertical are used. We also see convergence of parameters with horizontal resolution; however, high internal viscosity requires very fine horizontal resolution.

4. Results

Example solutions are presented in § 4.1 and § 4.2 to demonstrate the feasibility of the method. We then return to validate the non-dimensionalization used, and discuss the interpretation of solutions over the entire dimensionless parameter space.

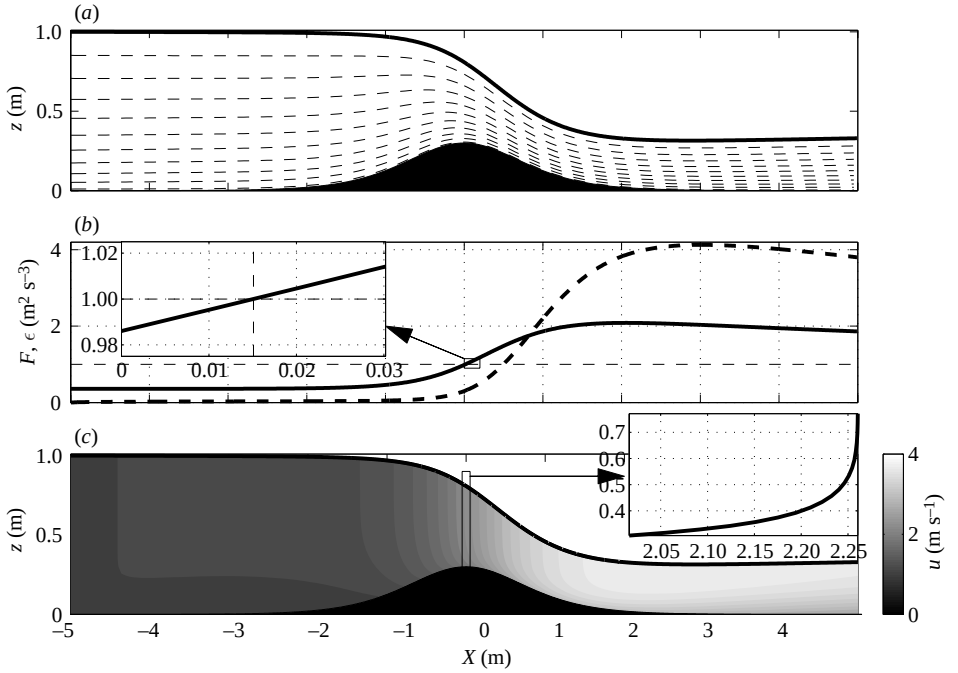

FIGURE 1. Sample solution ($\nu = 10^{-2}\,\mathrm{m^2\,s^{-1}}$, $C_d = 10^{-2}$), showing (*a*) layer height and streamlines; (*b*) Froude number (solid line), with inset highlighting the smooth behaviour of the Froude number at the control point and depth-averaged dissipation per unit mass (dashed line) as a function of X; (*c*) velocity field, with inset showing velocity profile at the control point.

4.1. *Specific solutions*

Figure 1 shows the solution for flow over a sill in a constant-width channel with viscosity $\nu = 0.01\ \mathrm{m^2\,s^{-1}}$ and dimensionless drag coefficient of $C_d = 0.01$. The fluid depth is $\eta_0 = 1\,\mathrm{m}$ at the upstream end and the upstream channel length is $L = 5\,\mathrm{m}$. The sill height is $H_s = 0.3\,\mathrm{m}$ and the sill half-width at half-maximum height is $\ell = 1\,\mathrm{m}$ (corresponding to $C_d/A \approx 0.07$ and $1/ReA \approx 0.04$). We use $N_X = 2 \times 10^4$ horizontal grid points.

The solution is similar to those for inviscid overflows – the layer plunges over the sill, and becomes supercritical near the sill top. However, the control point is 15 mm downstream of the sill (see inset in figure 1*b*). Dissipation per unit mass (panel *b*) is relatively small on the upstream side and increases in the lee of the sill, reaching a maximum 3 m downstream. The velocity field shows the acceleration of the fluid over the sill, and also highlights the development of vertical shear in the interior of the flow. The profile at the control (panel *c*, inset) is constant near the top of the water column, and sheared towards the lower boundary. This lower boundary layer thickens downstream of the sill, thereby reducing the Froude number.

We repeat the above calculation for a flat-bottomed channel that varies in width, rather than in depth. The constriction is half as wide as the full channel, and the results are shown in figure 2. This diagram shows that there are few qualitative differences between flow through a lateral contraction and flow over a sill. The layer accelerates through the constriction, and the control point is shifted downstream (although not

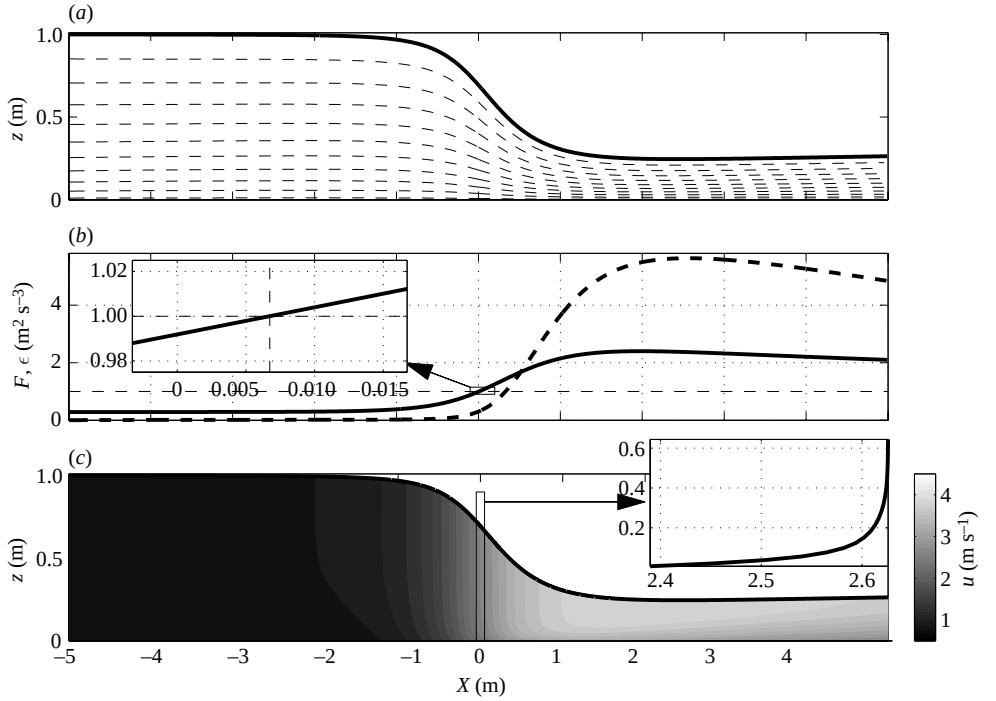

FIGURE 2. A solution with the same parameters as figure 1, but for a flat bottomed channel that varies in width, reaching a smooth minimum at $X = 0$.

as far as in figure 1). Most dissipation occurs downstream of the contraction, and the velocity shear is strongest near the lower boundary.

4.2. *Velocity distribution at the control point*

In the following experiments we use the channel geometry with a single sill (figure 1), and vary viscosity over the range $\nu = [10^{-6}, 0.25]\,\mathrm{m^2\,s^{-1}}$, keeping bottom drag constant $C_d = 0.01$ (or $1/ReA = [2.7 \times 10^{-6}, 0.68]$ and $C_d/A \approx 0.07$). The upper limit of this viscosity range is fixed by numerical resolution. In these experiments, horizontal resolution ($N_X = 2 \times 10^5$) is constant. There is no lower limit in viscosity, but it is shown below that flow is close to the inviscid solution at $\nu = 10^{-4}\ \mathrm{m^2\,s^{-1}}$.

Figure 3 shows velocity profiles (solid lines) at the control point over the viscosity range. When viscosity is low (e.g. figure 3*a*, where $\nu = 10^{-6}\,\mathrm{m^2\,s^{-1}}$) a thin bottom boundary layer forms, whereas the rest of the velocity profile is uniform. At intermediate values of viscosity the bottom drag influences a significant portion of the water column. At higher values of viscosity the whole water column is affected by the bottom drag, so that for $\nu \approx 0.25\,\mathrm{m^2\,s^{-1}}$ the profile is only weakly dependent upon depth. In other words, at very high or low values of viscosity the velocity profile is more slab-like; at intermediate values of viscosity the velocity profile is more curved.

These results are in stark contrast to the analytical solution of Garrett (2004), who assumes a balance between horizontal pressure gradients and viscous forces to derive velocity profiles at the control that are quadratic – these predicted profiles are shown in figure 3 by dashed lines, which in (*a*)–(*c*) are off scale. The assumption of a balance between internal friction and the horizontal pressure gradient at the control point is violated in all cases, including the highest viscosity case (figure 3*e*) where the

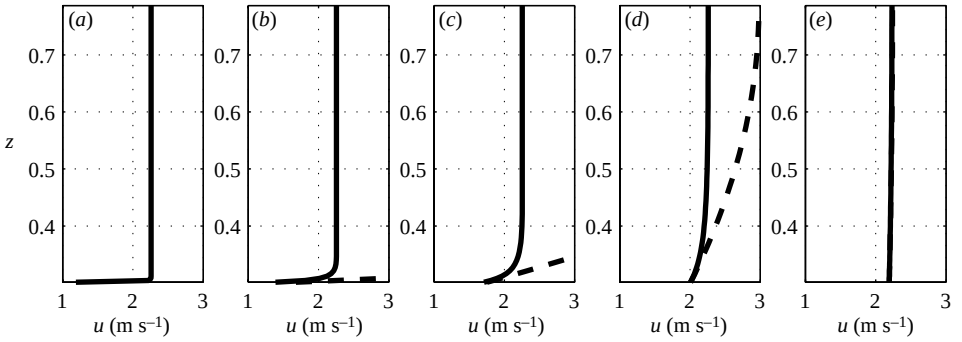

FIGURE 3. Velocity profiles at the control point with $C_d = 10^{-2}$ and channel geometry as for figure 1. Solid black lines show numerical solution, dashed lines show parabolic prediction (Garrett 2004). (*a*) $\nu = 10^{-6}\,\mathrm{m^2\,s^{-1}}$; (*b*) $\nu = 10^{-4}\,\mathrm{m^2\,s^{-1}}$; (*c*) $\nu = 10^{-3}\,\mathrm{m^2\,s^{-1}}$; (*d*) $\nu = 10^{-2}\,\mathrm{m^2\,s^{-1}}$; (*e*) $\nu = 0.25\,\mathrm{m^2\,s^{-1}}$.

quadratic prediction is accurate only because shear is negligible. While the primary balance of terms at the control (not shown) in every case is between inertia and buoyancy, viscosity throughout the flow influences the velocity profile and thus the control condition. Therefore, the solution requires knowledge of the time-history of each fluid parcel at the control point and simplifying assumptions about the dynamics are not applicable to the cases shown here.

4.3. *Channel aspect ratio*

The non-dimensional scaling which was introduced in § 2.3 can be tested by solutions for several aspect ratios A across $(1/ReA, C_d/A)$ space. In figure 4 we show such solutions with either $1/ReA$ fixed (panels a, b) or C_d/A fixed (panels c, d). Figure 4(a, c) shows the flux anomaly, which is defined relative to the flux q_i in the inviscid solution: $q^* = (q_i - Q\eta_0)/q_i$, while 4($b, d$) shows the dimensionless bottom slope at the control point.

These results clearly show that the lack of dependence on aspect ratio is consistent with the scaling proposed. The slight mismatch between some of the curves is consistent with enhanced dissipation levels above a sill that occupies a different fraction of the channel length (i.e. ℓ is held constant, but L increases as A is decreased). However, the data clearly indicate that the role of the sill width is secondary: the dominant horizontal length scale is the channel length over which velocity shear is generated, modifying both the control point and flux. Thus, in the dimensional simulations the effect of doubling channel length is the same as doubling both viscosity and bottom drag. In summary, while there appear to be three dimensionless parameters (Re, C_d and A) in the problem, this can be reduced to two parameters ($1/ReA$ and C_d/A) using the proposed scaling.

4.4. *Viscous hydraulics*

The numerical solutions to this problem can be found over a wide range of viscosity and bottom drag (and hence channel geometry). The range in viscosity is identical to that used in figure 3, corresponding to $1/ReA = [2.7 \times 10^{-6}, 0.68]$. The range in bottom drag for these experiments corresponds to $C_d/A = [7.1 \times 10^{-5}, 0.71]$. There is no lower limit on bottom drag, but there may be a physical upper limit where the sill slope is insufficient to allow control points to occur (e.g. we reach this limit at $C_d \approx 0.4$ for the sill shape used here).

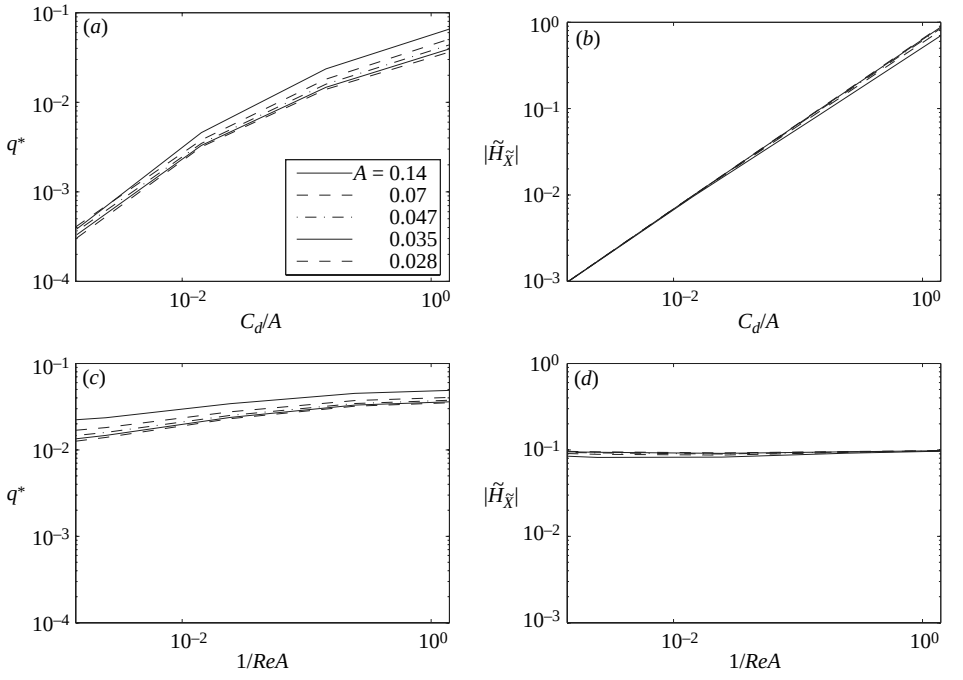

FIGURE 4. (*a*) Dimensionless flux anomaly q^*, and (*b*) dimensionless bottom slope at control point as a function of C_d/A for fixed $1/ReA$. (*c*) Dimensionless flux anomaly q^*, and (*d*) dimensionless bottom slope at control point as a function of $1/ReA$ for fixed C_d/A. Five lines are plotted for different values of aspect ratio A, demonstrating the accuracy of the scaling in (2.13) and (2.14).

We begin by showing as a function of effective viscosity $1/ReA$ and effective bottom drag C_d/A the flux made dimensionless by the inviscid flux: $\tilde{q} = Q\eta_0/q_i$ (figure 5*a*). Here the result is intuitive – both bottom drag and viscosity extract energy from the flow, and thus reduce the flux. In general, both of these quantities are required to make a significant impact on the flux. The maximum reduction of flux for the parameters used is about 17 % from the inviscid case.

The dimensionless flux data are plotted using logarithmic axes in figure 5(*b*). The qualitative result is not altered here: flux is a monotonic function of both $1/ReA$ and C_d/A. However, this diagram shows the relative contribution of each parameter in reducing the flux. For a given value of viscosity the flux decreases exponentially with bottom drag. If bottom drag is held constant, increasing viscosity can reduce the flux, but only to the point where the velocity becomes slab-like (see figure 3*e*). In short, the upper limit for flux reduction is set by the bottom drag, and the internal viscosity may perturb this flux.

The different roles of internal viscosity and bottom drag are further clarified by plotting the control position, as indicated by the dimensionless bottom slope at the control (figure 5*c*). Again, bottom drag dictates the position of the control point, and viscosity acts to perturb that position. For both very small and very large viscosity, the layer is slab-like (as shown in figure 3) so that the bottom drag sets the position of the control point to be downstream of the sill, as predicted by Pratt (1986) using the approximation of slab flow. While internal viscosity acts to shift the control point back towards the sill (i.e. closer to $X = 0$), matching the general conclusions of Garrett (2004), the shift is significant only at intermediate viscosities.

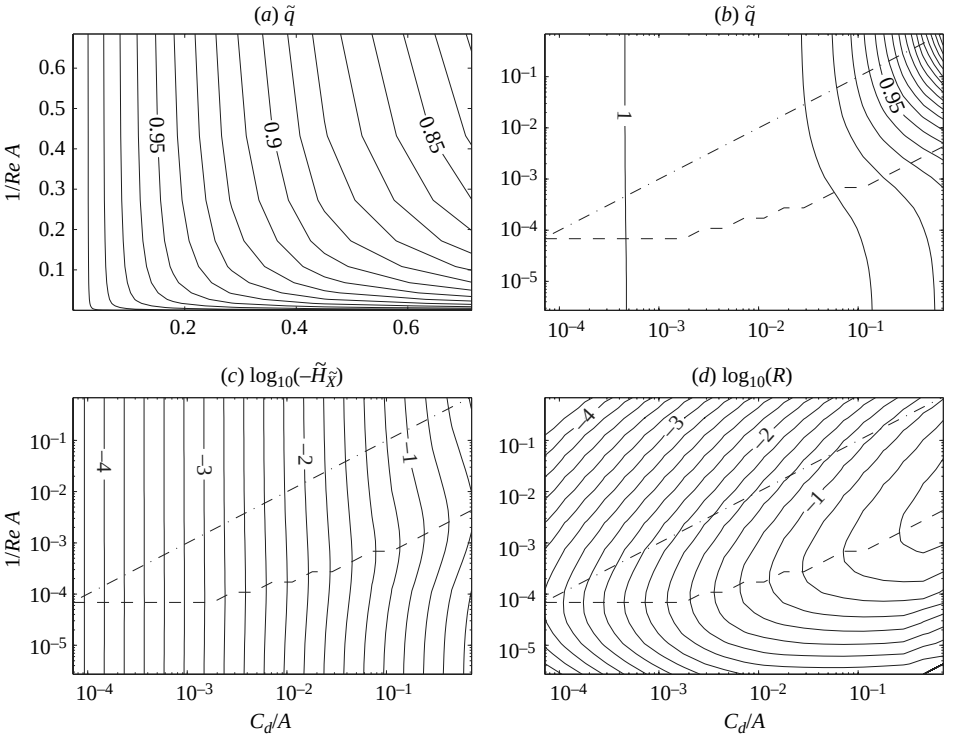

FIGURE 5. (*a*) Dimensionless flux $\tilde{q}$; (*b*) $\tilde{q}$ plotted with logarithmic axes; (*c*) the logarithm of the dimensionless bottom slope at the control point; and (*d*) the ratio R of viscous and bottom drag terms influencing the control position, as a function of $1/ReA$ and C_d/A. The dashed line in (*b*), (*c*) and (*d*) shows the position of the maximum relative contribution from internal dissipation, while the dash-dot lines show $1/ReA = C_d/A$.

We evaluate the relative influence on control position of internal dissipation and boundary drag using (2.11). For the case considered here (with $b_X = 0$) the ratio R of the two components is

$$R \equiv \left(\int_0^{\eta_0} \frac{2\nu u_\eta^2}{u^3 z_\eta} \, \mathrm{d}\eta \right) / C_d, \tag{4.1}$$

as was defined by Garrett (2004). The logarithm of R is plotted in figure 5(*d*), which shows that the primary influence on control position is due to bottom friction. Here, the maximum relative contribution from internal viscosity is shown by the dashed line. When internal viscosity is small, the flow is slab-like, and the control position is dictated by bottom drag so that control moves downstream. For high viscosity, the flow is also slab-like, and a similar value of R is found. Thus, the maximum effect of viscosity on the control point occurs for intermediate, and not extreme, values of viscosity (contrary to predictions based on Garrett's simplifying assumptions; see his figure 10). In addition, R does not approach unity for any of the cases investigated here, suggesting that the control point cannot be returned to the sill at any value of viscosity.

5. Discussion and conclusions

In this study we have artificially separated the effects of bottom drag and internal viscosity on a hydraulic flow. This separation permits comparison of results with

previous studies, and the development of physical intuition. However, in a real flow, internal viscosity and bottom drag are related. Take, for example, a fully turbulent open channel flow. This flow can be modelled using an eddy viscosity ν_t (assumed constant) which can be estimated using a mixing-length argument (Tennekes & Lumley 1972): $\nu_t \approx u'l$, where u' is the characteristic scale of the r.m.s. turbulent velocity fluctuation and l is the eddy length-scale. From Tennekes & Lumley (1972) we find that

$$C_d \sim 2\left(\frac{u'}{U}\right)^2$$

where U is the mean flow velocity. Furthermore, if we assume a balance between the local rates of production $P \sim -\overline{u'w'}\partial U/\partial z$ and dissipation $\epsilon = 2\nu_m \overline{s_{ij}s_{ij}}$ of turbulent kinetic energy, we obtain

$$P \sim u'^2\frac{U}{h} \sim \epsilon \sim \frac{u'^3}{l},$$

where $s_{ij} = \partial u_i'/\partial x_j$ represents the small-scale velocity gradients and ν_m is the molecular viscosity (Tennekes & Lumley 1972). Thus, we can estimate the eddy viscosity in terms of bottom drag:

$$\nu_t \sim C_d U h. \tag{5.1}$$

This is similar to the expression used by Garrett (2004). Equation (5.1) is an order of magnitude argument, but does provide us with a means of estimating the relative magnitudes of these quantities. Therefore, using the non-dimensional scaling we expect $1/ReA \sim C_d/A$, as shown by the dash-dot line in figure 5. The velocity profile of an example close to satisfying this condition is shown in figure 3(*d*).

This study also provides a sound physical basis upon which to derive and interpret the Froude number (2.9). This definition can be compared with the Froude number and critical condition defined by Nielsen, Pratt & Helfrich (2004) for a continuously stratified, weakly viscous and diffusive flow over a sill:

$$\overline{F}^2 \equiv \frac{\overline{u}^2}{\overline{g'}h} = \frac{\beta}{\alpha}, \tag{5.2}$$

where $\overline{u}$ is the mean velocity in the flowing layer, $\overline{g'}$ the mean reduced gravity and α and β are 'shape coefficients' calculated from velocity and density profiles, respectively. The velocity shape coefficient is defined to be

$$\alpha = \frac{\displaystyle\int_H^{H+h} u^2 \,\mathrm{d}z}{h\overline{u}^2}, \tag{5.3}$$

while $\beta = 1$ for the unstratified case considered here. Although the condition (5.2) was derived assuming conditions of self-similarity, it was found to hold to a good approximation in numerical simulations of continuously stratified flow with a free-slip bottom boundary. If we calculate (5.2) in the present study, the control condition becomes

$$\alpha\overline{F}^2 = \frac{\displaystyle\int_H^{H+h} u^2 \,\mathrm{d}z}{gh^2} = 1, \tag{5.4}$$

which differs substantially from (2.9). Equations (2.9) and (5.4) are equivalent only when

$$\frac{1}{h^2}\int_H^{H+h} u^2\,\mathrm{d}z \int_H^{H+h} u^{-2}\,\mathrm{d}z = 1. \tag{5.5}$$

Expanding (5.5) about the mean velocity (and assuming that $(\alpha-1) \ll 1$) demonstrates that this condition is satisfied only when $\alpha = 1$ (i.e. u does not vary with height).

The Froude number criterion derived by Nielsen *et al.* (2004) is exact only when the flow is self-similar. The possibility of self-similar hydraulic solutions has been demonstrated for inviscid stratified flows (Wood 1968; Engqvist & Hogg 2004), but exact self-similarity is prohibited by the inclusion of friction (Garrett 2004). For the case investigated here, the only self-similar solution is the trivial one in which u is constant with height. However, in the reduced gravity case considered by Nielsen *et al.* (2004), stratification may be sufficiently strong that the self-similar solution (while not exact) provides a good estimate of control position. It follows that an extension of the numerical technique used here to the continuously stratified case may help to resolve conditions under which the self-similar condition is relevant – but this is well beyond the scope of the current paper.

The numerical solution for viscous hydraulic flow presented here demonstrates two important points. First, Garrett's (2004) conclusion – that increasing bottom drag shifts the control point downstream of the topographic constriction, whereas increasing internal viscosity tends to return the control back upstream – is confirmed. However, the effect of internal viscosity on the control point is second order when compared with the effect of bottom drag, and it cannot restore the control position back to the topographic constriction. Second, we find that the relative influence of internal dissipation on the control position is maximum at an intermediate value of viscosity. This occurs because the flow is slab-like at both large and small viscosity, and the effect of internal dissipation on the control position is proportional to the integrated square of the velocity shear.

The shape of the velocity profile at the control is sensitive to the flow viscosity and bottom drag. The profiles depend upon both the physical parameters governing the control position and the path history of each fluid parcel. This demonstrates that the addition of viscosity to hydraulic theory removes the length-independence which is often used to enable analytical solutions for these nonlinear flows. It follows that future expansion of this numerical solution method (to multiple density layers and bidirectional flow) will also need to integrate over the entire domain in order to find relevant solutions.

Chris Garrett kindly provided comments and suggested improvements on the first two drafts of this manuscript. Karl Helfrich and an anonymous referee also helped to substantially improve the paper. Our thanks also to Peter Killworth and Ross Griffiths who commented on a draft manuscript. A. M. H. is supported by an Australian Research Council Postdoctoral Fellowship (DP0449851).

REFERENCES

Armi, L. 1986 The hydraulics of two flowing layers with different densities. *J. Fluid Mech.* **163**, 27–58.

Engqvist, A. & Hogg, A. M. 2004 Unidirectional stratified flow through a non-rectangular channel. *J. Fluid Mech.* **509**, 83–92.

Garrett, C. 2004 Frictional processes in straits. *Deep-Sea Res.* II **51**, 393–410.

Garrett, C. & Gerdes, F. 2003 Hydraulic control of homogeneous shear flows. *J. Fluid Mech.* **475**, 163–172.

Gill, A. E. 1977 The hydraulics of rotating-channel flow. *J. Fluid Mech.* **80**, 641–671.

Hogg, A. M., Ivey, G. N. & Winters, K. B. 2001 Hydraulics and mixing in controlled exchange flows. *J. Geophys. Res.* **106**, 959–972.

Killworth, P. D. 1992 On hydraulic control in a stratified fluid. *J. Fluid Mech.* **237**, 605–626.

Nielsen, M. H., Pratt, L. & Helfrich, K. 2004 Mixing and entrainment in hydraulically driven stratified sill flows. *J. Fluid Mech.* **515**, 415–443.

Pratt, L. J. 1986 Hydraulic control of sill flow with bottom friction. *J. Phys. Oceanogr.* **16**, 1970–1980.

Tennekes, H. & Lumley, J. L. 1972 *A First Course in Turbulence*. The MIT Press.

Wood, I. R. 1968 Selective withdrawal from a stably stratified fluid. *J. Fluid Mech.* **32**, 209–223.